JOURNAL OF CATALYSIS **134**, 204–219 (1992)

Microstructure of Rh–Ce Particles on Silica: Interactions between Ce and SiO_2[1]

K. R. KRAUSE,[2] P. SCHABES-RETCHKIMAN,* AND L. D. SCHMIDT[3]

*Department of Chemical Engineering and Materials Science, University of Minnesota, Minneapolis, Minnesota 55455; and *Instituto de Fisica, UNAM Apdo. Postal 20-364, México, D.F. 01000, Mexico*

Received August 20, 1991; revised October 18, 1991

We have characterized the microstructure of Rh/Ce on SiO_2 after heat treatments in H_2 and O_2 using TEM, HREM, XPS, and EELS, focusing on the very stable structures formed after heating in H_2. After initial reduction at 600°C, Rh is present as 50- to 100-Å metal particles while the Ce forms a uniform amorphous film of Ce^{3+} on the SiO_2. After oxidation at 600°C, Rh is oxidized to Rh_2O_3 and spreads over the SiO_2 surface while Ce forms small patches and large (>1000 Å) particles of crystalline CeO_2. After reduction of the oxidized microstructure at 600°C, Rh metal returns with a less uniform particle size distribution, while Ce is reduced to Ce^{3+} and structures indicating strong interactions between Ce and Si are formed. Upon reduction in the presence of Rh, the CeO_2 particles are reduced to crystalline $Ce_2Si_2O_7$ as confirmed by HREM. The Ce silicate nucleates at Rh particles and spreads over the support as large thin (>1000 Å diameter and ~50 Å thick) single-crystal patches. After reoxidation at 650°C, both Ce silicate (Ce^{3+}) and CeO_2 were identified using EELS chemical shifts, indicating that the crystalline silicate, once formed, is stable in oxygen. Ce on SiO_2 also showed interaction between Ce and Si, but no crystalline species formed after reduction and only small crystalline CeO_2 particles formed after oxidation. Thus, the formation of the Ce silicate and the oxidation of Ce to CeO_2 are catalyzed by Rh. This work represents the first direct evidence for the formation of a Ce silicate in this system, and the combined use of HREM, XPS, and micro-EELS permits chemical characterization of these structures. © 1992 Academic Press, Inc.

INTRODUCTION

Rh and Ce are major components in the automotive exhaust catalyst. Rh is mainly responsible for the reduction of NO_x, while Ce is added in large amounts as a reaction promoter and for support stabilization. On silica, Ce addition to Rh has been shown to improve the selectivity for oxygenates (*1*) and increase the overall rate of CO hydrogenation (*2*) but does not affect the rate of ethane hydrogenolysis (*2*). On alumina, adding large amounts of Ce to Rh improved both the selectivity toward N_2 (*3*) and the reaction rate for CO + NO (*3, 4*). Also, CO oxidation activity by Rh was enhanced after Ce addition by reducing the negative-order inhibition effect of CO (*5, 6*). Evidence for the formation of a Ce aluminate in Rh/Ce on alumina spheres during heat treatment in H_2 at 900°C has been found using X-ray absorption (*7*). H_2 chemisorption measurements indicated that Ce increased the dispersion of Rh on silica but had no effect on alumina (*4*).

We have previously examined the microstructure of Rh/Ce on SiO_2 with TEM and electron diffraction (*2*) and typical results are summarized in Fig. 1. When heated in H_2 (Fig. 1A), a thin continuous film of partially reduced cerium formed on the SiO_2. The only observed effect of Ce addition on the Rh particles was that Rh/Ce on SiO_2 exhibited more defects and less faceting than Rh only on SiO_2. Heating in O_2 (Fig. 1B) oxidized the Rh to Rh_2O_3 and caused the Ce film to coalesce, forming many small CeO_2 patches and some large, flat (>1000 Å diam-

[1] This research sponsored by NSF under Grants CBT-882745 and INT-9000511.

[2] Supported by a National Science Foundation Graduate Fellowship.

[3] To whom correspondence should be addressed.

0021-9517/92 $3.00
Copyright © 1992 by Academic Press, Inc.
All rights of reproduction in any form reserved.

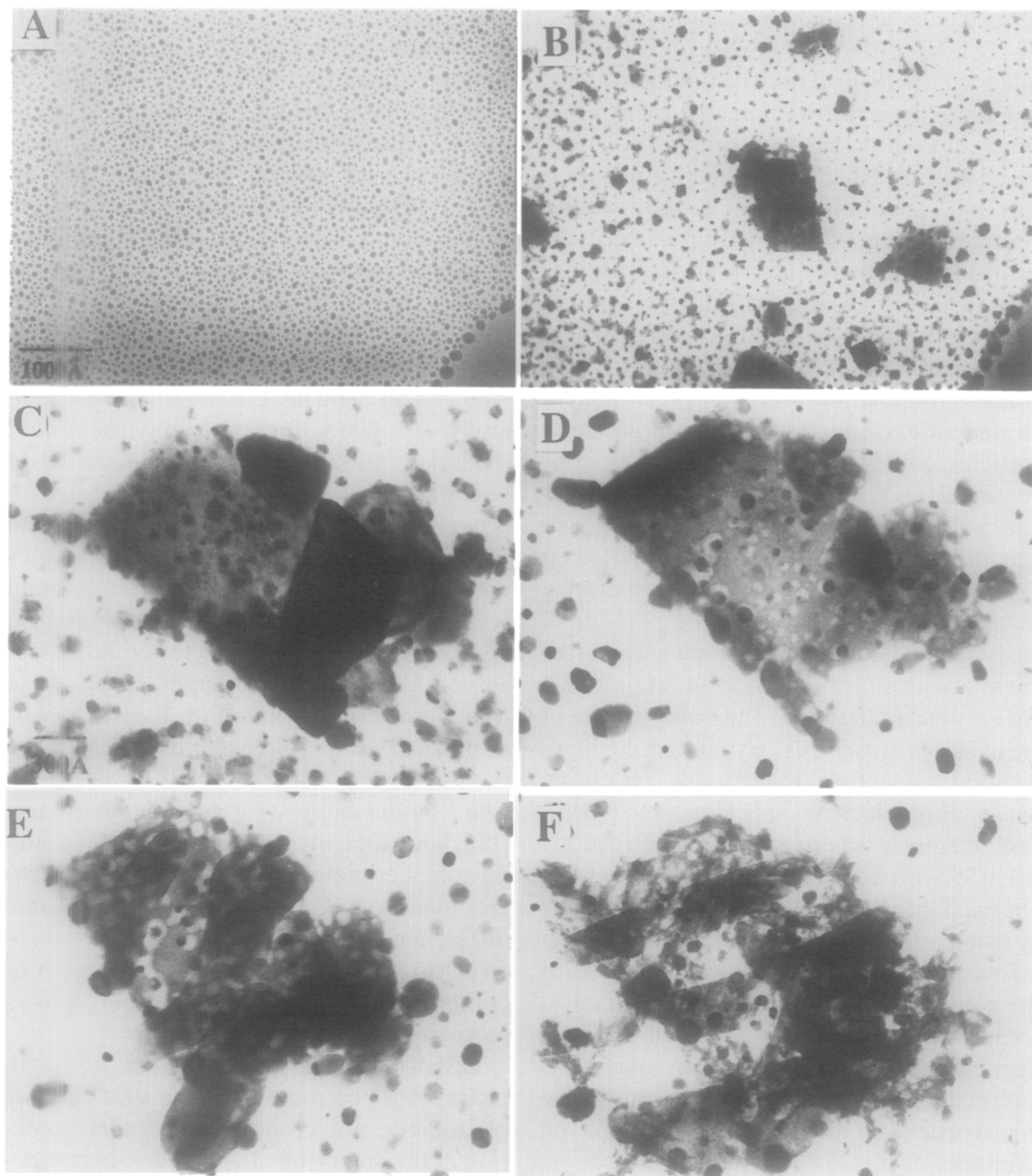

FIG. 1. Micrographs of Rh/Ce on SiO_2. (A) after heating in H_2 at 600°C. Rh is present as metal particles and Ce forms a thin film on the SiO_2. (B) After heating in O_2 at 650°C. Rh is oxidized to Rh_2O_3 and Ce forms many small patches and several large particles of CeO_2. (C) Higher magnification image of the large CeO_2 particle in the center of (B). After successive heatings in H_2 for (D) 20 h at 600°C, (E) 58 h at 650°C, and (F) 22 h at 750°C. The large particle is not completely dispersed after reduction for 100 h (*2*).

eter and ~100 Å thick) CeO_2 particles. Upon reduction in H_2 at 600–700°C, the larger CeO_2 particles were observed to disperse very slowly and form very stable structures, possibly by interacting with the SiO_2. The large CeO_2 particle in the center of Fig. 1B is shown after oxidation in Fig. 1C and its transformation into very stable "fingers"

after extensive reduction is shown in Figs. 1D–1F. Note that the small CeO_2 patches compose the majority of the microstructure and that these are completely reduced to the Ce film after the first reduction. It was observed that Rh catalyzes both the oxidation and reduction of the Ce. After initial treatment in H_2, the Rh particles were observed to be mostly uniform in size. Oxidation–reduction cycling with Ce present resulted in a much less uniform Rh particle size distribution.

The composition of the stable fingers formed after reduction of the large CeO_2 particles could not be determined by conventional TEM because no electron diffraction pattern was observed. We proposed that they may involve interaction between Ce and Si, possibly by the formation of a Ce silicate. We have now used a combination of analytical techniques to further characterize the microstructure of Rh/Ce on SiO_2, focusing on determination of the composition of these stable structures. By combining high-resolution electron microscopy (HREM), X-ray photoelectron spectroscopy (XPS), and electron energy loss spectroscopy (EELS) with conventional TEM, we have obtained information that was not available by using a single technique. EELS measurements in a TEM allowed determination of the valence state of Ce and of the chemical composition from areas as small as 30 Å diameter. We are also currently using this multitechnique approach to characterize the microstructures of Rh/Ce and Pt/Ce on alumina.

EXPERIMENTAL

TEM sample preparation has been described in detail elsewhere (2). An amorphous SiO_2 film (~200 Å thick) was prepared on a gold TEM grid by depositing Si on formvar and heating to 800°C to decompose the formvar and convert the Si to amorphous SiO_2. Thin films (~20 Å) of Rh and Ce were vacuum deposited on top of the SiO_2, and the grid was heated in H_2 at 600°C for 4 h to disperse the Rh film into particles. Multiple loadings were prepared on the same grid by selectively shielding regions of the grid during evaporations. This allowed preparation of several different Rh/Ce ratios, along with an internal standard region of Rh only to check for possible contamination during heat treatments on a single TEM grid.

Samples were treated in a quartz tube furnace with high-purity H_2 or O_2 flowing at ~50 cc/min. The heat treatments were generally at ~600°C for ~4 h in a reduction, oxidation, and rereduction sequence. TEM was performed on a Philips CM30 microscope equipped with a parallel detection EELS system. The same regions of samples could be treated, examined, retreated, and reexamined so that the morphological changes of individual particles could be observed. Typical micrographs after these treatments are shown in Fig. 1. HREM was performed on a JEOL 4000EX TEM using the same samples used in EELS and TEM. The "model catalysts" we have characterized here and in previous work generally have higher metal loadings and larger particles than "real" powder catalysts and some differences may exist between the microstructures. The $Rh/Ce/SiO_2$ system is very complicated and the planar support allows more complete characterization.

EELS was performed using a Gatan model 666 spectrometer with a 1024 channel photodiode array, allowing parallel detection of the spectrum. Typical low-loss spectra were acquired in 1–2 min and core-loss spectra in ~5–10 min. The electron dispersion was typically ~0.3 eV/channel and could be varied between 0.1 and 4.0 eV/channel. The incident electron beam energy was 300 keV except for some thickness measurements and low-loss spectra when it was reduced to 100 or 200 keV. The energy resolution measured by the FWHM of the zero-loss peak was <2 eV at 300 keV when using small entrance apertures to the spectrome-

ter. Spectra were acquired in both TEM image mode and diffraction mode depending on the information desired. Low-loss spectra were acquired with a spatial resolution of ~30 Å by using a magnification of 370,000 in image mode and a 1-mm spectrometer aperture. The collection angle β was limited to 10 mrad by insertion of an objective aperture. Core-loss spectra for EELS microanalysis were usually acquired in diffraction mode with a 2-mm spectrometer aperture from a ~100-Å-diameter area. Spectra acquired from the carbon K edge region (~285 eV) showed no evidence of C contamination and are not shown.

In ideal situations the elemental composition of small areas can be determined by low-loss EELS. The most obvious method for analyzing a small area is to condense the beam to a small spot. By doing this, spots as small as ~50 Å can be obtained and spectra can be acquired from only the area illuminated by the incident beam. Contamination and/or beam damage can result from this method since the incident intensity is very high in a very localized area. The second method involves performing EELS in the image mode at high magnification and small spectrometer entrance apertures. An area of diameter $d = d_s/M$, where d_s is the spectrometer entrance aperture diameter and M is the magnification, is imaged at the spectrometer (*8*). Thus, if $d_s = 1$ mm and $M = 370{,}000$, the area analyzed is ~30 Å in diameter. Contamination and beam damage are minimized and selection of the desired small area is easier. All low-loss spectra shown here were acquired by the second method.

Thickness measurements were made from low-loss spectra by determining the ratio I_t/I_0, where I_t is the integrated intensity of the entire spectrum and I_0 is the integrated intensity of the zero-loss peak. The natural logarithm of this ratio equals t/λ, where t is the thickness of the area from which the spectrum was acquired and λ is the inelastic mean free path (*8*). The program NTLAMBDA by Zaluzec was used to calculate λ within ~20% (*9*).

XPS samples for analysis of Rh/Ce on SiO_2 were prepared by heating Si wafers in O_2 to oxidize the top ~500 Å to SiO_2 while minimizing charging. Three samples were then prepared by vacuum evaporating 20 Å Rh (Rh alone), 20 Å Ce (Ce alone), and 20 Å each of Rh and Ce (Rh/Ce) on top of the SiO_2. Samples were heated together sequentially in H_2 at 600°C, H_2 at 800°C, O_2 at 600°C, O_2 at 600°C, H_2 at 600°C, H_2 at 800°C, and O_2 at 600°C. Each treatment lasted 4 h in pure H_2 or O_2 flowing at ~50 cm³/min. After each treatment, XPS spectra were acquired by transferring the sample in air at room temperature to a PHI 5400 spectrometer.

Peak energies were calibrated against adventitious carbon at 284.6 eV. All other multiplex spectra were shifted by the same energy difference (0 to ~6 eV). Peak positions measured after correction of charging for Rh, Ce, Si, and O were internally consistent (i.e., the O and Rh peaks from Rh_2O_3 appeared at the correct binding energies when Rh_2O_3 was formed), indicating that differential charging was not significant.

The valence state of the Ce can be determined by the peak positions and features of the 3*d* XPS spectra. Ce^{4+} has a peak at 918-eV due to ionization to an excited $3d_{3/2}$ state (*10*). This peak is absent in Ce^{3+} or lower valence spectra. The Ce^{4+} and Ce^{3+} spectra have two doublet peaks split by 18 eV centered around 885 and 903 eV. In Ce^{4+}, the lower binding energy component of each doublet is the most intense, while the opposite is observed for Ce^{3+}. Ce metal also has peaks at these energies, but is easily identified by the absence of the doublets. The valence state of the Ce can be determined by analyzing these qualitative features of the Ce 3*d* spectra.

XPS on many Si–O compounds showed that the binding energy of the Si 2*p* line of 15 natural silicates is about 1 eV less than that of SiO_2 (*11*). Also, the binding energy

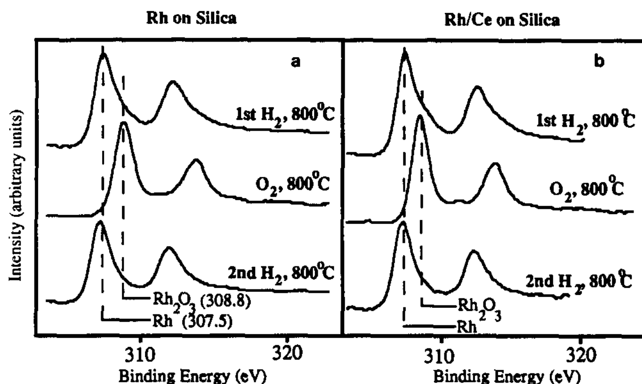

FIG. 2. Rh $3d$ XPS spectra (a, Rh on SiO_2; b, Rh/Ce on SiO_2) during a sequence of treatments in H_2 and O_2. Both sets of spectra show that Rh is present as Rh metal after heating in H_2 and is oxidized to Rh_2O_3 after heating in O_2.

of the O $1s$ line was found to be 0.7 eV less for silicates than for SiO_2. These values are indicated on the spectra and, in the absence of literature data for $Ce_2Si_2O_7$, were used as estimates of the binding energies for this silicate.

RESULTS

XPS

XPS spectra of the Rh $3d$, O $1s$, Si $2p$, and Ce $3d$ transitions taken after H_2 and O_2 treatments for 4 h at the temperatures indicated are shown in Figs. 2–5, respectively.

Rh/SiO₂. The behavior of Rh alone on SiO_2 was as expected (Figs. 2a, 3a, 4a) (*12*). After heating in H_2, Rh is present as Rh metal, and O and Si are present as SiO_2. Small peaks due to Rh_2O_3 are observed in the Rh and O spectra. After heating in O_2 at 600°C, the Rh is completely oxidized to Rh_2O_3 as evidenced by the Rh and O spectra. No change was observed in the Si. Reduction of the oxidized sample in H_2 reforms Rh metal on SiO_2. The oxidation and reduction of Rh is complete after the first 600°C treatment in O_2 or H_2, respectively. The Si spectra after each treatment were identical, both in width and in binding energy, indicating that SiO_2 in the presence of Rh is unaffected by treatment in H_2 and O_2 at these temperatures.

Ce/SiO₂. XPS spectra of Ce alone on SiO_2 are shown in Figs. 3b, 4b, 5a. After heating in H_2 at 800°C, Ce is nearly completely reduced to Ce^{3+}. Only a small peak is visible at 918 eV, which is probably due to room-temperature oxidation of the sample while being transported from the oven to the spectrometer. Spectra acquired after heating in H_2 at 600°C showed a mixture of Ce^{3+} and Ce^{4+}, but after heating in H_2 at 800°C only small amounts of Ce^{4+} remained. The Ce is completely oxidized to Ce^{4+} after heating in O_2 at 600 and 800°C. Reduction in H_2 at 800°C transforms the Ce back to Ce^{3+}.

The O $1s$ spectra show multiple oxygen containing species. After heating in H_2 at 800°C two overlapping peaks were observed. The higher peak is close to the binding energy of SiO_2. The more intense lower peak is clearly not from CeO_2; rather it is from partially reduced Ce in the form of Ce_2O_3 or a Ce silicate. After oxidation, peaks from CeO_2 and SiO_2 are observed. The SiO_2 peak increases in intensity after oxidation. XPS is highly surface sensitive with a penetration depth of ~20 Å and the Si signal increase is due to decreased cover-

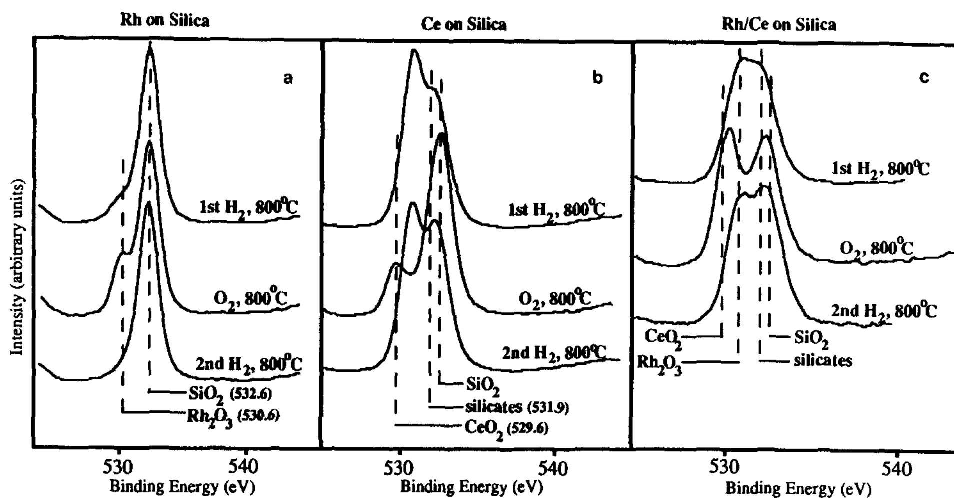

FIG. 3. O 1*s* XPS spectra (a, Rh on SiO_2; b, Ce on SiO_2; c, Rh/Ce on SiO_2) during sequence of treatments in H_2 and O_2.

age of the SiO_2 surface by the Ce film. This is consistent with the TEM observations (Fig. 1) since in H_2 the silica is covered by a Ce-containing film and in O_2 the Ce coalesces into CeO_2 particles exposing the silica surface. After reduction at 800°C, the O 1*s* spectrum returns to that after the first reduction. No significant differences were observed, and the SiO_2 peak decreased in intensity relative to the lower binding energy peak.

The Si 2*p* XPS spectra from Ce only on SiO_2 show that Si interacts strongly with the Ce. After both treatments in hydrogen at 800°C, the Si peak broadens and shifts to lower energy due to the formation of another

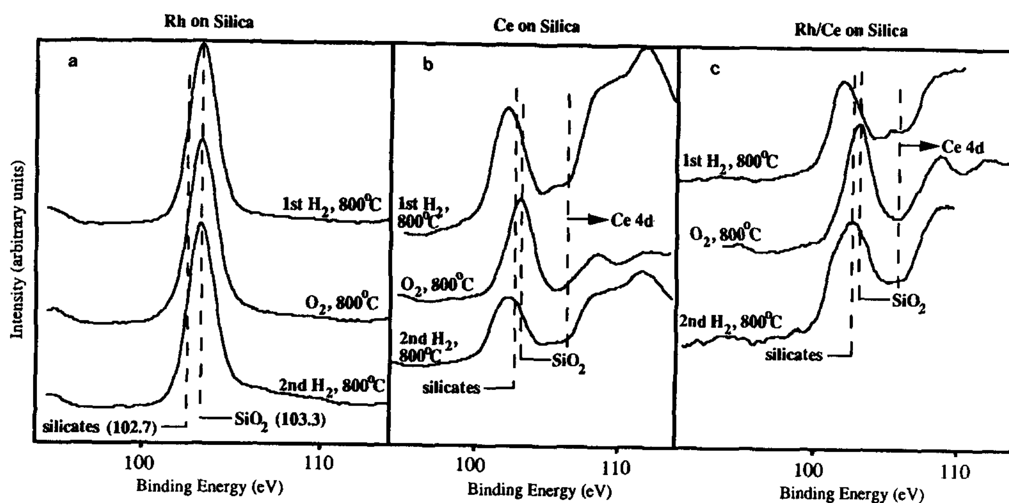

FIG. 4. Si 2*p* XPS spectra (a, Rh on SiO_2; b, Ce on SiO_2; c, Rh/Ce on SiO_2) during sequence of treatments in H_2 and O_2. No change from SiO_2 is observed for Rh only, but there is a strong interaction between Ce and SiO_2 after heating in H_2.

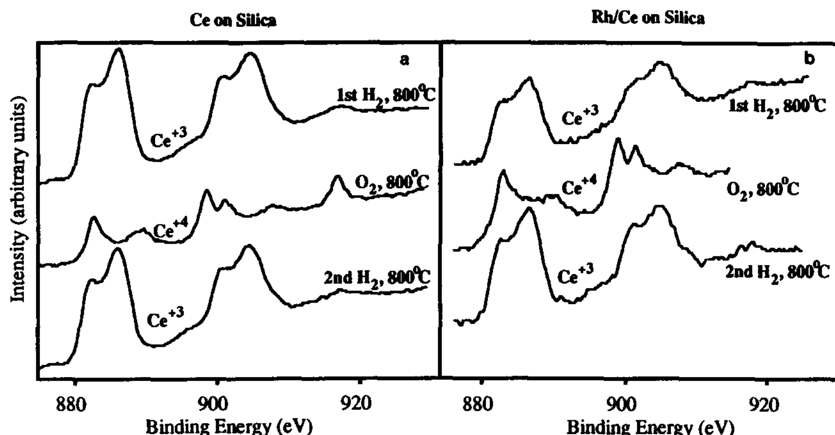

FIG. 5. Ce 3*d* XPS spectra (a, Ce on SiO_2; b, Rh/Ce on SiO_2) during sequence of treatments in H_2 and O_2. Ce is transformed between 3+ and 4+ valence states by treatment in H_2 and O_2, respectively.

Si-containing species. The magnitude of the shift is not nearly enough to indicate reduction of the SiO_2 to elemental Si (99 eV), but is consistent with the formation of a silicate. After oxidation, the Si peak narrows and returns to the binding energy of SiO_2. This behavior is in sharp contrast to that observed for Rh on SiO_2 where no changes in the Si spectra were observed. The features around 110-eV binding energy are due to the 4*d* state of Ce. Subtraction of X-ray satellites from the Ce 4*d* states confirms that these do not contribute significantly to the Si 2*p* peaks.

Rh/Ce/SiO₂. The results for Rh/Ce on SiO_2 (Figs. 2b, 3c, 4c, 5b) show no evidence for the formation of species containing both Rh and Ce. After all treatments in H_2, Rh is present as Rh metal with a small shoulder at higher binding energy due to Rh_2O_3. The Rh is oxidized to Rh_2O_3 after heating in O_2.

The O 1*s* spectra after heating in H_2 are similar to those observed for Ce only on SiO_2 except that the changes in microstructure are catalyzed by Rh. The spectrum observed after initial heating in H_2 at 600°C with Rh present is very similar to that observed after heating at 800°C without Rh. After oxidation, the high-binding-energy peak shifts to the position of SiO_2 while the low-energy peak is a composite of Rh_2O_3 and CeO_2. After reduction at 600°C, the observed spectrum is again very similar to that of Ce only after reduction at 800°C.

The Si 2*p* spectra from Rh/Ce only on SiO_2 are very similar to those observed for Ce only. After each treatment in H_2, the Si peak is broadened and shifted to slightly lower energy than SiO_2 indicating that the SiO_2 is interacting with the Rh and Ce and is consistent with the formation of a silicate. After oxidation, the peak narrows and returns to the binding energy of SiO_2. As with Ce only on SiO_2, the features around 110-eV binding energy are due to the 4*d* state of Ce, and contributions from X-ray satellites of these features to the Si spectra are insignificant.

The Ce 3*d* spectra of Rh/Ce on SiO_2 show that Ce is transformed between 3+ and 4+ valence states. After both treatments in H_2 at 800°C, Ce is present as Ce^{3+}. Heating in O_2 oxidizes the Ce to CeO_2. The spectra are very similar to those observed for Ce only on SiO_2 except that reduction from 4+ to 3+ is more complete after heating at 600°C with Rh present.

Thus, XPS of Rh only on SiO_2 showed that Rh transforms between Rh metal and Rh_2O_3 while the *SiO_2 was unchanged*. The

same Rh behavior was observed when Ce was present; however, the *SiO_2 was found to interact with the Ce*. Ce was present in the 3+ valence state after treatment in H_2 and as CeO_2 after oxidation. XPS results also indicate that the reduction of Ce is catalyzed by Rh.

EELS

The TEM results indicate the presence of stable "blobs" or fingers after heating in H_2 (Fig. 1), and XPS shows that there are chemical shifts accompanying these changes (Figs. 2–5). However, while XPS has a ~10-Å depth resolution as indicated by attenuation and reappearance of Si peaks, XPS has no lateral resolution and merely measures the average oxidation state over the entire surface. Therefore, EELS was used to obtain chemical information from selected areas of Rh/Ce on SiO_2 as small as 30 Å in diameter.

Low-loss micro-EELS. In the energy range 0–50 eV, EELS spectra have peaks due to plasmon excitations of the compounds, and we show that these can be used for analysis with ~30-Å lateral resolution. Ce has two peaks at 13 and 32 eV, Rh has a single peak at 24 eV, and the thin SiO_2 support has no significant peaks. The Rh and Ce peak energies are indicated in Figs. 6–8.

The thickness of the SiO_2 was estimated by low loss spectra acquired from several areas of the sample with no Rh and Ce to be 100 Å (see Fig. 8c). The thickness was very uniform over the areas examined and varied by less than 10 Å. Figure 6 shows low-loss spectra from three areas (labeled A, B, and C) after treatment in H_2 at 650°C for 4 h. Spectrum A is from the ~150-Å-diameter particle and clearly shows intensity at the Rh plasmon and Rh $N_{2,3}$ energies. Contributions from small amounts of Ce are also present in this spectrum as can be seen from increases in slope at the Ce plasmon energies and the small increase in intensity at the Ce $N_{4,5}$ energy. These results agree well with TEM observations of the microstructure after heating in H_2, which show metallic Rh particles and a thin film of Ce. Assuming the particle was Rh metal, is thickness was estimated as ~100 Å. Spectra B and C are from different particles on the support and are similar to the spectrum from A except the Rh features are not as intense. The thickness of the ~100-Å-diameter particles B and C was estimated as ~60 Å.

The low-loss spectra after heating the same sample in O_2 at 650°C for 4 h are shown in Fig. 7. After oxidation, all three particles labeled as a, b, and c contain Ce, in agreement with diffraction results that identified them as CeO_2. No Rh particles were identified by low-loss EELS after oxidation, confirming TEM results indicating that the Rh migrates over the SiO_2 surface. A slight increase in intensity at the Rh $N_{2,3}$ energy was observed in many spectra (most obvious in a) suggesting that the Rh is being transported by the Ce. This is a possible mechanism for the redispersion of the Rh after O_2–H_2 cycling. By assuming the particles to be CeO_2, their thicknesses were estimated to be 90 Å for a and ~40 Å for b and c.

Low-loss spectra after heating the same sample in H_2 at 650°C for 4 h are shown in Fig. 8. EELS shows that the particle labeled a is a 125-Å-thick Rh particle, while the patch labeled b contains Ce. By assuming the patch to be $Ce_2Si_2O_7$, its thickness was estimated to be 30 Å. The silica support contributes only slightly to the low-loss spectrum as shown by c.

Large area core loss EELS. Ce M_{45} ($3d$) core-loss EELS spectra from large areas (>1000 Å) of the Rh/Ce samples after the initial reduction, after oxidation, and after the second reduction are shown in Fig. 9. TEM micrographs are very similar to those in Figs. 6–8 and are not shown. The Ce M_{45} edge has two sharp peaks, called white lines, due to a high density of unfilled f-states (*8*), which allow accurate measurement of chemical shifts. After both reductions, the maxima of the white line peaks were at 883.5 and 900.3 eV. No Ce phases were detected by electron diffraction, but the valence state

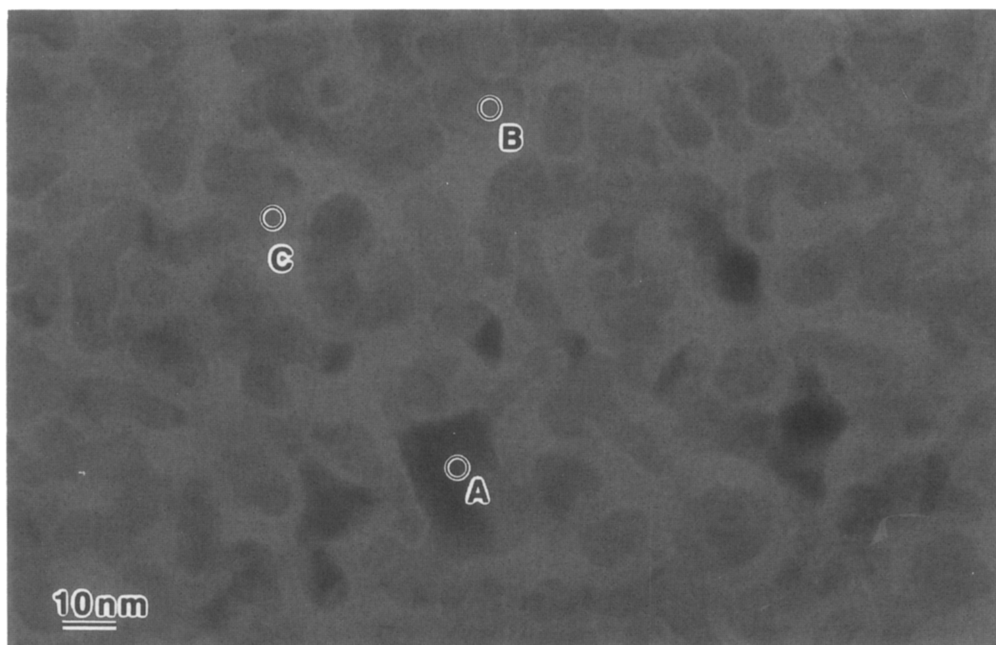

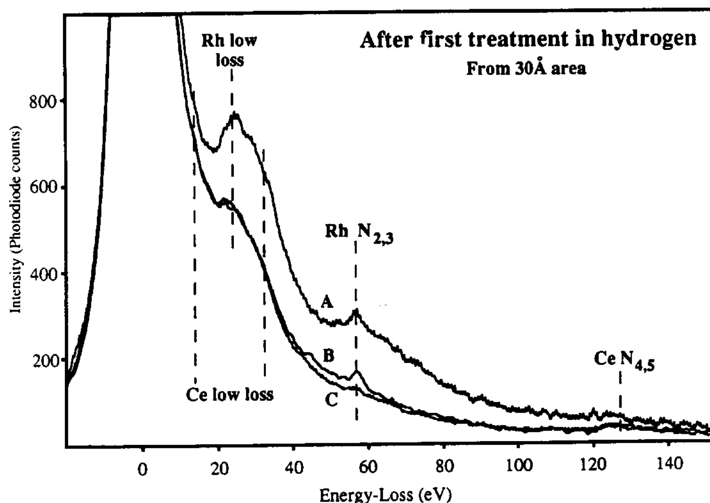

FIG. 6. TEM micrograph and EELS low-loss spectra of Rh/Ce on SiO_2 after initial heating in H_2 at 650°C for 4 h. The spectra labeled A, B, and C are from the respective areas of the micrograph and show Rh with small amounts of Ce.

of Ce was determined to be 3+ by XPS over a large area. The spectrum observed after oxidation was from CeO_2, identified by electron diffraction and XPS, and the white line maxima were at 885.0 and 902.0 eV. The observed shift in the higher-energy peak of 1.7 eV corresponds to transformation of the Ce between 3+ and 4+ valence states. The spectra were acquired and calibrated identically, and the measured energies were reproducible to ±0.3 eV over experiments on several samples. Note also that, similar to XPS, the spectra after oxidation and reduction treatments are qualitatively different.

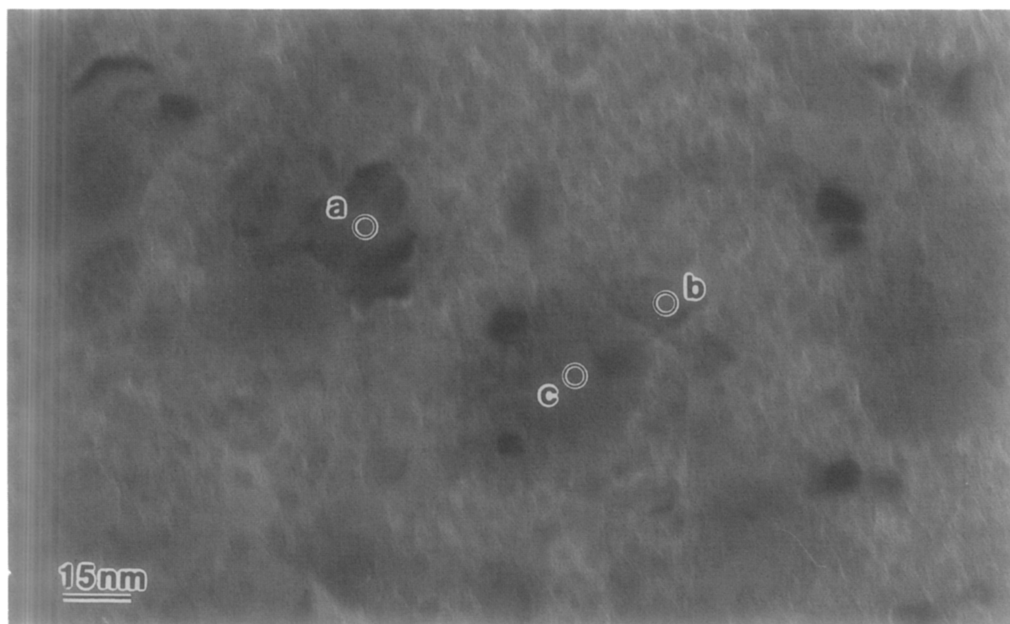

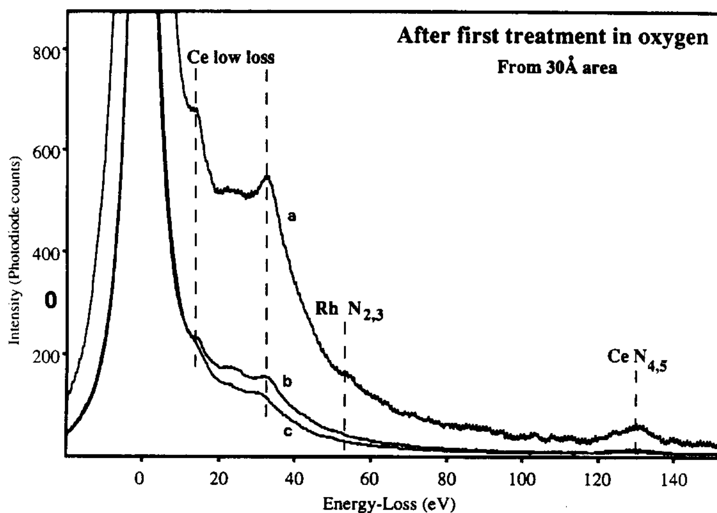

FIG. 7. TEM micrograph and EELS low-loss spectra of Rh/Ce on SiO_2 after heating in O_2 at 650°C for 4 h. The spectra labeled a, b, and c are from the respective areas of the micrograph and show Ce possibly with small amounts of Rh.

The 4+ spectrum has a significant and reproducible high-energy shoulder that is absent from the 3+ spectra. Also, the higher-energy white line of the 4+ spectrum is more intense than the lower-energy line, but the reverse is true for the 3+ spectrum. These features were used to aid identification of the valence state and do not require precise measurement of the white line energies.

Micro-core-loss EELS. One of the powerful advantages of EELS over XPS is the ability to obtain chemical information with very high lateral resolution. This is illus-

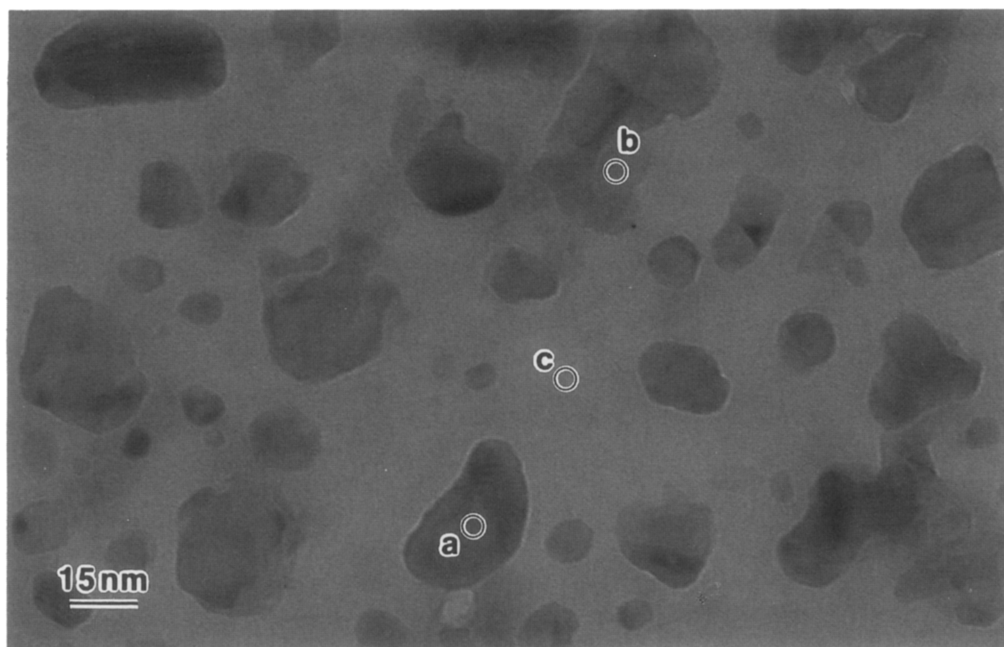

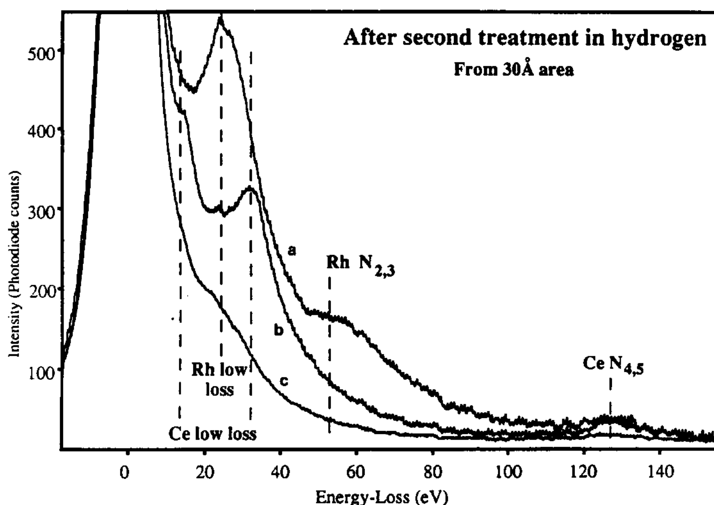

FIG. 8. TEM micrograph and EELS low-loss spectra of Rh/Ce on SiO_2 after the second treatment in H_2 at 650°C for 4 h. The spectra labeled a, b, and c are from the respective areas of the micrograph and show regions of Rh, Ce, and only SiO_2.

trated by Fig. 10, which shows Ce $M_{4,5}$ spectra from ~100-Å-diameter areas of the same sample after reoxidation at 650°C for 4 h. Ce^{3+} and Ce^{4+} were detected *in the same sample* after oxidation. White line energies of the spectra labeled a and b are 883.2 and 900.0 eV, indicating Ce^{3+}. The areas a and b in the micrograph are Ce silicate that, under these oxidation conditions, is stable against reoxidation to CeO_2. The majority of the areas show spectra like those of c and d. The white line energies of 884.8 and 901.8 eV, along with the appearance of high-energy shoulders,

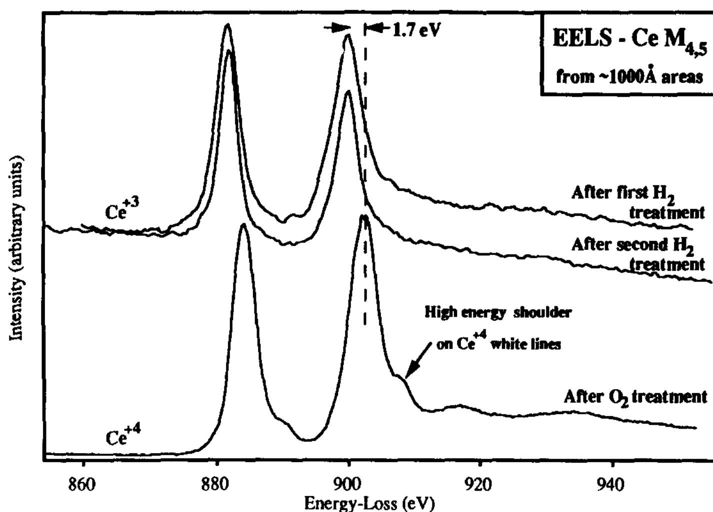

FIG. 9. Ce $M_{4,5}$ EELS spectra acquired from ~1000 Å areas of Rh/Ce on SiO_2 after initial reduction, oxidation, and second treatment in H_2 all at 650°C for 4 h. A shift of 1.7 eV in white line energies was measured between the H_2 was measured between the H_2 and O_2 treatments. Also, note the high-energy shoulders on the oxidized spectra. The spectra correspond to Ce valence states of 3+ after reduction and 4+ after oxidation.

indicate Ce in the 4+ valence state. Electron diffraction identified these regions as CeO_2.

HREM

HREM was performed on samples that had been reduced, oxidized, and then rereduced to further characterize the very stable patches that form after this heat treatment sequence. Typical regions are shown in Figs. 11 and 12. The features observed in the micrographs are identified from contrast, atomic spacings, and EELS microanalysis. The very low-contrast background of the micrographs is due to the amorphous SiO_2.

The highest contrast particles are Rh (labeled Rh in Figs. 11 and 12). The 200-Å-diameter particle in the center of Fig. 11 shows a white dot pattern with spacings of 2.20 Å (111) and 1.90 Å (200) between rows rotated by 54°, indicating that the [110] plane is parallel to the surface. Lattice fringes and atom rows can also be seen in the large Rh particle in the lower left of Fig. 12. Some faceting is observed, although the Rh particles are generally irregular in shape.

The crystalline regions extending away from the Rh particles are the very stable patches (see Fig. 1) that were previously identified as amorphous by electron diffraction. These large (patches >1000 Å were observed), thin (<~50 Å from the contrast and EELS measurements) crystalline patches were observed covering a significant fraction of the surface. No crystalline regions were observed in Ce-only samples that underwent identical heat treatments as the Rh/Ce samples. Their formation is observed only in samples containing both Rh and Ce, and they are always observed extending away from one or more Rh particles, indicating that *Rh catalyzes their nucleation and growth*. Several of the patches are observed to *grow underneath Rh particles*. For example, note the patches on the right center, left center, and the small patches on the upper center of Fig. 11. The fringes are observed to continue unaffected into (under) the Rh particles, indicating that they are at constant height relative

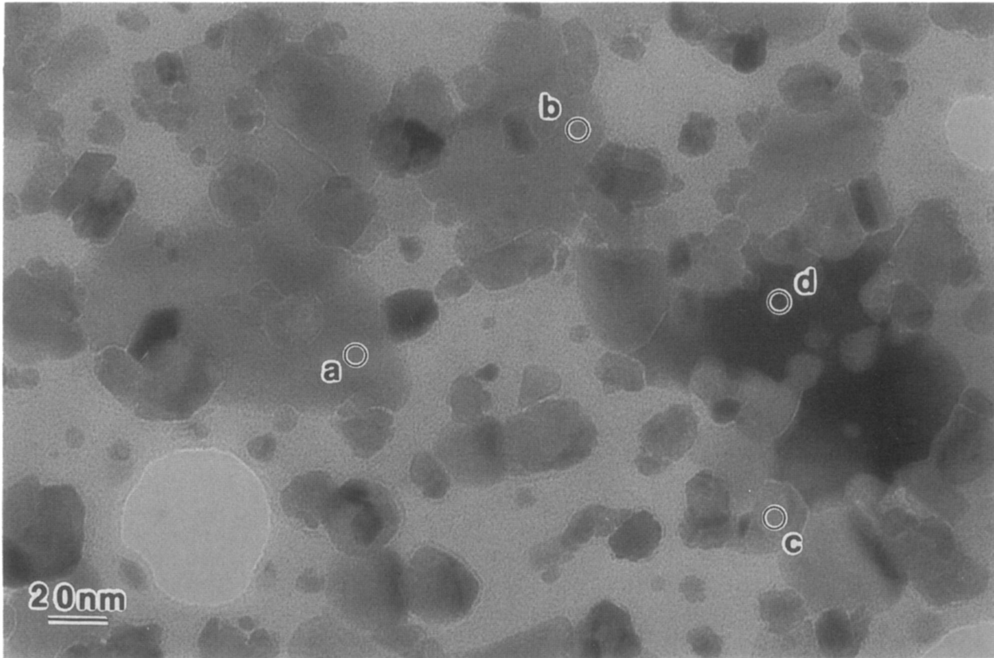

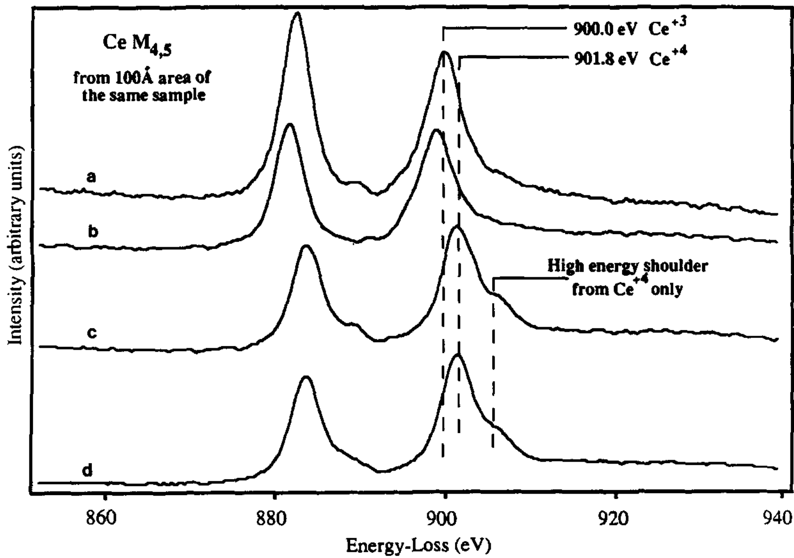

FIG. 10. TEM micrograph and Ce $M_{4,5}$ EELS spectra from Rh/Ce on SiO_2 after H_2–O_2–H_2–O_2 treatments. Spectra a, b, c, and d are from the respective areas labeled in the micrograph. Regions a and b contain Ce^{3+}, while regions c and d *in the same sample* contain Ce^{4+}.

to the SiO_2 surface. If the patches were on top of the Rh, then their images would change due to changes in focus.

Lattice spacings of several patches (labeled Ce) were measured. The patch on the left side of Fig. 12 shows a zipper-like pattern with large periodicity spacings of 13 Å. This patch is bounded on the right by another patch, which extends to a nearby Rh particle. Spacings of 8.7 and 5.4 Å were also

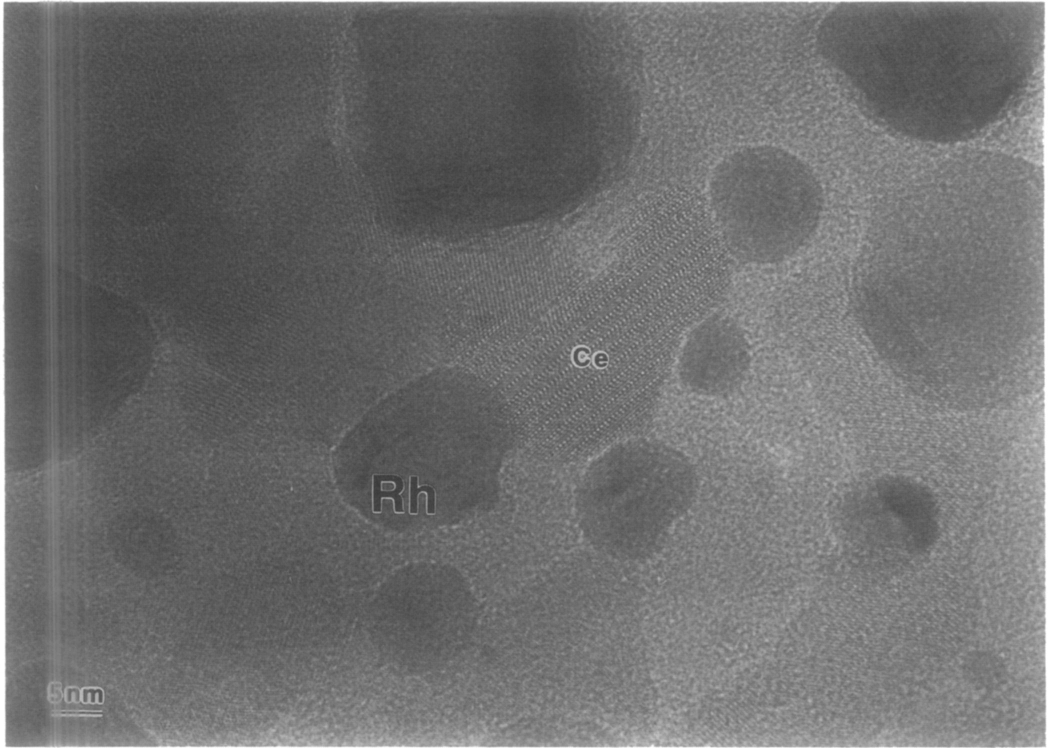

FIG. 11. HREM micrograph taken after second treatment in H_2 showing several Rh particles and crystalline $Ce_2Si_2O_7$ patches.

observed, in addition to smaller spacings. These agree well with the Ce silicate $Ce_2Si_2O_7$, which is orthorhombic with lattice constants of $a = 8.722$ Å, $b = 13.056$ Å, and $c = 5.401$ Å (*13*). Search of the literature revealed no other phases consistent with the measured spacings, particularly the unusually large spacing of 13 Å. The zipper-like pattern shown on the left side of Fig. 12 is typical of a multielement species with large differences in atomic number, consistent with the silicate since it is composed of low atomic number Si (14) and O (8) and high atomic number Ce (58).

DISCUSSION

The microstructure of this system is shown schematically in Fig. 13. After the initial H_2 treatment, Ce forms a thin uniform film on the SiO_2. This film contains Ce^{3+} and XPS showed interaction between Ce and SiO_2, although no crystalline Ce phases are formed. After oxidation, Ce forms small CeO_2 particles over most the sample. These are easily transformed back to a Ce^{3+} film by heating in H_2. Some large CeO_2 particles are also formed by heating in O_2, however, and these are reduced to $Ce_2Si_2O_7$ by treatment in H_2.

The large, thin blobs previously observed (*2*) with TEM after heating Rh/Ce on SiO_2 in H_2 have been shown by XPS and EELS to be Ce^{3+} with shifts in Si indicating silicates and by HREM to be single-crystal $Ce_2Si_2O_7$. These patches were very stable against further reduction in H_2 and their well-defined edges indicated that they were not simply patches of Ce dispersing back into a uniform film.

XPS shows that there is strong interaction between Ce and SiO_2 after heating in H_2, which produces a binding state of Si consis-

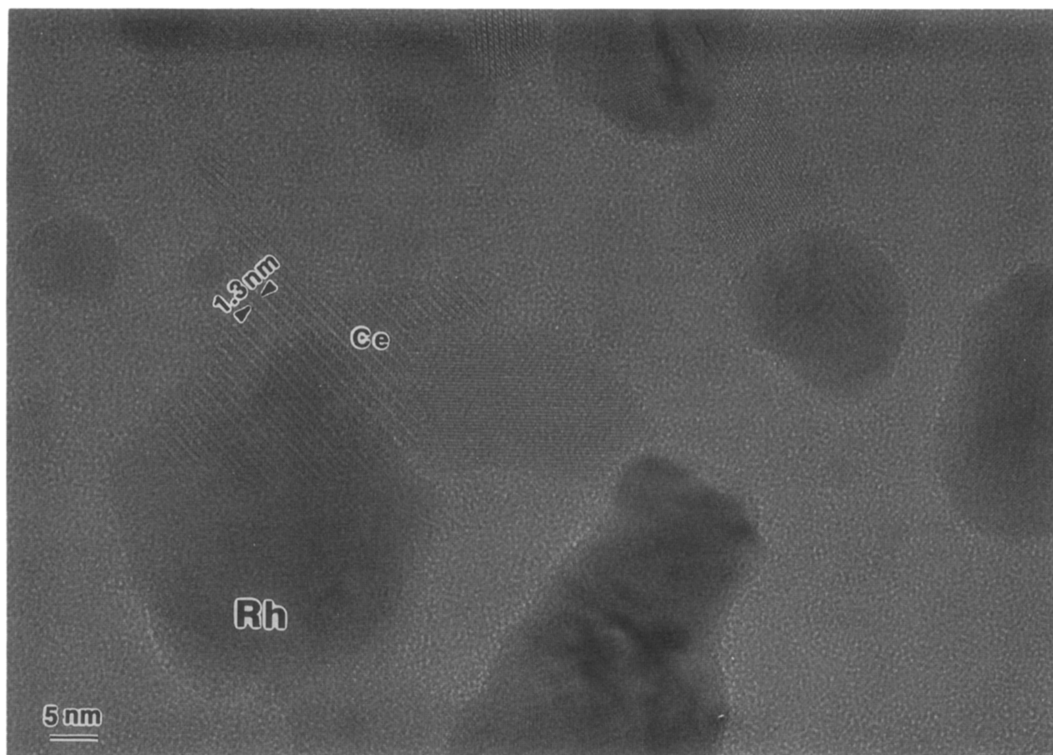

FIG. 12. HREM micrograph taken after second treatment in H_2 showing $Ce_2Si_2O_7$ patch underneath Rh particle. The silicate is only observed in contact with Rh particles.

tent with formation of a silicate. This interaction was not observed for Rh only on SiO_2. In addition, heating in H_2 reduced the Ce to Ce^{3+} consistent with the silicate $Ce_2Si_2O_7$. No evidence that Rh forms compounds with the Ce or Si was observed.

The high lateral resolution of EELS was used to show that the patches formed after reduction contain Ce in the 3+ valence state. Low-loss EELS from individual patches indicated the presence of Ce and the absence of significant amounts of Rh. The valence state was determined by measurements of chemical shifts in and changes in shape of the Ce $M_{4,5}$ core loss edge. The observation by EELS of Ce^{3+} and Ce^{4+} in the same sample after heating in O_2 (Fig. 10) showed that the patches of Ce^{3+}, once formed, are stable against oxidation up to 650°C.

Direct identification of the patches as $Ce_2Si_2O_7$ was provided by HREM. Figure 11 and particularly Fig. 12 clearly show that the patches are large single crystals adjacent to and sometimes underneath Rh particles. D-spacing measurements identified the patches as $Ce_2Si_2O_7$. The crystals were not detected previously (*2*) by electron diffraction, both because they are very thin and because the more intense low-order diffraction spots or rings are obscured by the broad rings of the amorphous SiO_2. Some lower intensity higher-order rings may have been observed, which we suggested could indicate the presence of Ce hydride, although further characterization has shown no evidence of Ce hydride.

Previous studies of the crystal structure of the silicate $Ce_2Si_2O_7$ found that it could be formed by heating fine powders of CeO_2

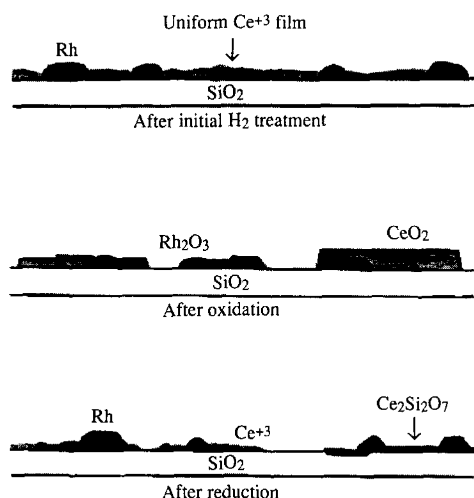

FIG. 13. Schematic of the microstructure of Rh/Ce on SiO_2 after reduction and oxidation. Many small CeO_2 particles are formed by heating in O_2 and these are reduced to a Ce^{3+} film by heating in H_2. Some large CeO_2 particles that are reduced to $Ce_2Si_2O_7$ by treatment in H_2 are also formed.

and SiO_2 at 1500°C in an inert atmosphere or under high vacuum (*13*). CeO_2 was reduced to Ce_2O_3 and simultaneously formed $Ce_2Si_2O_7$. Much lower temperatures (600–800°C) were used in the present work, and samples were heated in pure H_2. Also, the CeO_2 in these samples is in intimate contact with the SiO_2 film making nucleation easier. This may explain the observation of SiO_2 interaction with Ce in samples without Rh. Small amounts of Ce silicate may form as very small crystals or amorphous particles. The presence of Rh catalyzes the formation of the large particles of crystalline silicate. O_2 and H_2 are each adsorbed dissociatively on Rh and O and H atoms can migrate from the Rh to adjacent Ce catalyzing the formation of larger CeO_2 particles in O_2 and their reduction in H_2. As a result, large crystalline silicate patches are formed adjacent to Rh particles.

SUMMARY

We have used XPS, EELS, and HREM to characterize the formation of $Ce_2Si_2O_7$ in Rh/Ce on SiO_2 after heating in H_2 at 600–800°C, which forms large (>1000 Å), thin (~50 Å) patches adjacent to and under Rh particles. Rh acts as a catalyst for this process, probably by dissociatively adsorbing H_2, which then migrates as H atoms to reduce Ce^{4+} to Ce^{3+}. EELS was used to measure chemical shifts of the Ce directly from areas as small as 30 Å. Both Ce^{3+} and Ce^{4+} were observed with EELS after heating samples containing Ce silicate in O_2 at 650°C, indicating that the silicate is at least partially stable to oxidation at this temperature.

ACKNOWLEDGMENTS

The assistance of Dr. R. A. Caretta in performing the XPS and that of Luis Rendon in performing the HREM are greatly appreciated. P.S.-R. acknowledges support from CONACyT and DGAPA-UNAM 102789.

REFERENCES

1. Kiennemann, A., Breault, R., Hindermann, J.-P., and Laurin, M., *J. Chem. Soc. Faraday Trans. 1* **83,** 2119 (1987).
2. Chojnacki, T., Krause, K., and Schmidt, L. D., *J. Catal.* **128,** 161 (1991).
3. Oh, S. H., *J. Catal.* **124,** 477 (1990).
4. Klemmer, P. G., M.S. thesis, Brigham Young University, 1989.
5. Yung-Fang, Y. Y., *J. Catal.* **87,** 152 (1984).
6. Oh, S. H., and Eickel, C. C., *J. Catal.* **112,** 543 (1988).
7. Beck, D. D., Capeheart, T. W., and Hoffman, R. W., *Chem. Phys. Lett.* **159,** 207 (1989).
8. Egerton, R. F. "Electron Energy-Loss Spectroscopy in the Electron Microscope." Plenum Press, New York, 1986.
9. Zaluzec, N. J., *Ultramicroscopy* **28,** 283 (1989).
10. Burroughs, P., Hamnett, A., Orchard, A. F., and Thornton, G., *J. Chem. Soc. Dalton Trans.*, 1686 (1976).
11. Carriere, B., *et al., J. Electron Spectros. Relat. Phenom.* **10,** 85 (1977).
12. Wang, T., and Schmidt, L. D., *J. Catal.* **71,** 411 (1981).
13. Felsche, J., and Hirsiger, W., *J. Less Common Met.* **18,** 1131 (1969).